

Tuning-Free Amodal Segmentation via the Occlusion-Free Bias of Inpainting Models

Jae Joong Lee, Bedrich Benes, Raymond A. Yeh
Department of Computer Science, Purdue University
{lee2161, bbenes, rayyeh}@purdue.edu

Abstract

Amodal segmentation aims to predict segmentation masks for both the visible and occluded regions of an object. Most existing works formulate this as a supervised learning problem, requiring manually annotated amodal masks or synthetic training data. Consequently, their performance depends on the quality of the datasets, which often lack diversity and scale. This work introduces a tuning-free approach that repurposes pretrained diffusion-based inpainting models for amodal segmentation. Our approach is motivated by the “occlusion-free bias” of inpainting models, i.e., the inpainted objects tend to be complete objects without occlusions. Specifically, we reconstruct the occluded regions of an object via inpainting and then apply segmentation, all without additional training or fine-tuning. Experiments on five datasets demonstrate the generalizability and robustness of our approach. On average, our approach achieves 5.3% more accurate masks over the state-of-the-art.

1. Introduction

Amodal segmentation refers to predicting segmentation masks even under occlusions [25]. This challenging task involves reasoning about the unseen portion of an object under complex occlusion and illumination scenarios. It is an important problem with potential applications in autonomous driving and robot planning, which require reasoning beyond what is directly observed to predict possible future events in the environment [5, 12, 51].

Following the success of deep segmentation methods [3, 21, 30, 41], amodal segmentation is often formulated as a supervised learning task, i.e., a dataset of (image, amodal mask) pairs is collected to train a model. However, preparing a large dataset for amodal segmentation is challenging. Annotating amodal masks requires reasoning over occluded reason, which may be difficult and inconsistent among human annotators. Furthermore, scaling the diversity of the dataset is challenging as it requires numerous combinations

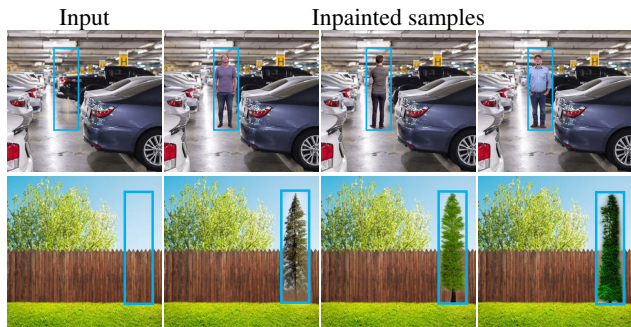


Figure 1. **Occlusion-free bias for a diffusion inpainting model.** We observe that an inpainted object is always placed without occlusions inside the inpainting area (blue box), e.g., a tree could have been inpainted behind the fence.

of occluders and objects.

Inevitably, several amodal segmentation methods turn to synthetically generating occlusions [1, 10, 34, 49] and 3D game engine rendering [18] to obtain the annotations. However, the performance is still limited by (a) the distribution gap between the synthetic and real data and (b) the size of the dataset. For example, the currently available SOTA [34] uses only 800k data pairs for training/fine-tuning, which is relatively small compared to the recent internet-scale datasets for other tasks [35, 36, 40]. Another work [50] also proposes to use a pre-trained diffusion model, but it requires iterative occlusion removal and is constrained to a fixed 83 object categories, which has limited generalizability.

To address these challenges, we present a *tuning-free approach* that utilizes existing foundation models trained on internet-scale datasets. Our method **does not require** any amodal data. Hence, the method is naturally zero-shot and without restriction to pre-defined object classes. Our approach is motivated by the observation that diffusion inpainting models have an “occlusion-free bias”, i.e., the inpainting model prefers to generate a whole object rather than the occluder given a reasonable mask as shown in Fig. 1. We propose to perform inpainting over an enlarged modal mask, where the diffusion model fills the oc-

cluded regions. With the inpainted occluded regions, we extract the modal segmentation as the amodal prediction.

We demonstrate the effectiveness of our approach on five diverse amodal segmentation datasets, namely, COCO-A [62], BSDS-A [61], KINS [37], FishBowl [45], and SAILVOS [18]. Notably, our tuning-free approach outperforms the current supervised SOTA [34] by an average of 5.3% in the mIoU.

Our contributions are as follows:

- We propose a tuning-free method for amodal segmentation (zero-shot) by exploiting the occlusion-free bias of diffusion inpainting models.
- The method involves several novel components, including a context-aware approach to background composition using RGB distribution, a noising process image for conditioning, and a modal mask construction procedure.
- We demonstrate the generalizability of the proposed method by conducting extensive experiments over four diffusion inpainting models on five diverse datasets.

2. Related Work

Amodal perception and segmentation. Humans can often detect and identify an object even if it is (partially) occluded [23]. Seminal work by Li and Malik [25] begins the line of work of using deep learning for amodal tasks. Many architectures and models have been proposed, *e.g.*, CNN [25, 49, 51, 60], Generative Adversarial Networks [8], Transformer [11, 46], and Diffusion-based models [34, 59]. Existing works are evaluated on datasets such as COCO-A [62], BSDS-A [61], KINS [37], and MP3D-Amodal [59], which consist of common objects from the real world. Other synthetic benchmarks are also popular, *e.g.*, SAILVOS [18] or FishBowl [45]. These synthetic datasets provide more diverse object categories and precise amodal mask annotations without human errors.

The current SOTA in amodal segmentation that involves training are pix2gestalt [34] and AmodalWild [59]. We refer to pix2gestalt as the SOTA as its code is ultimately released, whereas AmodalWild did not release the training code. pix2gestalt [34], which trains a deep-net to predict the occluded pixels following an analysis by synthesis framework [56]. Specifically, they created a synthetic amodal dataset by occluding objects with randomly sampled overlays using another object. Our work does not require any amodal datasets, *i.e.*, it is tuning-free.

Next, the closest related to our work is the tuning-free method proposed by Xu et al. [50], where they propose to iteratively use an inpainting modal for amodal completion, *i.e.*, they are interested in high image quality. Nonetheless, as a modal mask can be extracted from the completed image, we consider it to be an amodal segmentation method. The key limitation of Xu et al. [50], upon reviewing their code [20], is that the approach leverages class information

and is limited to only 83 classes his greatly limits the usability of their approach. In contrast, our method does not have class restrictions and does not require multiple calls to the inpainting model.

Image inpainting is the task of filling in missing regions of a given image, where the missing region is indicated using a mask. Early works in inpainting leverage low-level properties of natural images, *e.g.*, smoothness [6, 47] or low-rank [13, 19], to tackle this task. In cases where the image contains a large missing region, then generative or learning-based methods are proposed [14, 24, 26, 28, 53–55, 57]. More recently, diffusion models have emerged as the state-of-the-art in image generation, naturally, image inpainting methods based on diffusion have also been proposed [4, 29, 31, 40, 42, 44]. This work leverages pre-trained diffusion inpainting models for the tasks of zero-shot amodal segmentation, *i.e.*, we do not require high image quality, only accurate object contours.

Tuning-free methods for diffusion models. A diffusion model requires training on a large number of images to generate a realistic output. Although pre-trained diffusion models exist, fine-tuning is still needed for new tasks. Recent tuning-free methods leverage pre-trained models for performance gains and other tasks without extra training, improving Text-to-Image synthesis [7, 58] and video generation [15, 38]. Our approach aligns with these works as we do not require additional fine-tuning. Differently, this paper focuses on using pre-trained inpainting models for the *task of amodal segmentation*, and the method is tuning-free.

3. Preliminaries

We review diffusion models [17] and inpainting with diffusion [31]. Diffusion models add noise to the data (forward process) and learn to undo the added noise (reverse process) during training. At generation, diffusion models start from a purely sampled noise and perform the reverse process.

Forward diffusion process gradually adds Gaussian noise to a clean image, x_0 , over T timesteps where x_t is the noisy version of the image at timestep t with α_t controlling the amount of noise added at each step. The noisy image x_t can be computed from x_0 as follows

$$x_t = \sqrt{\bar{\alpha}_t}x_0 + \sqrt{1 - \bar{\alpha}_t}\epsilon \tag{1}$$

where $\bar{\alpha}_t = \prod_{s=1}^t \alpha_s$ is the cumulative product of the noise scaling factors and $\epsilon \sim \mathcal{N}(0, I)$ is a Gaussian noise.

Reverse diffusion process undoes the forward diffusion by denoising an image iteratively, starting from a pure noise image, x_T to the clean image, x_0 . This is formulated as a sequence of conditional probabilities

$$p_\theta(x_{t-1} | x_t) = \mathcal{N}(x_{t-1}; \mu_\theta(x_t, t), \sigma_t I) \tag{2}$$

following the Gaussian distribution with mean $\mu_\theta(x_t, t)$, and diagonal covariance matrix predicted from a deep-net with parameters θ . Intuitively, μ_θ can be thought of as act-

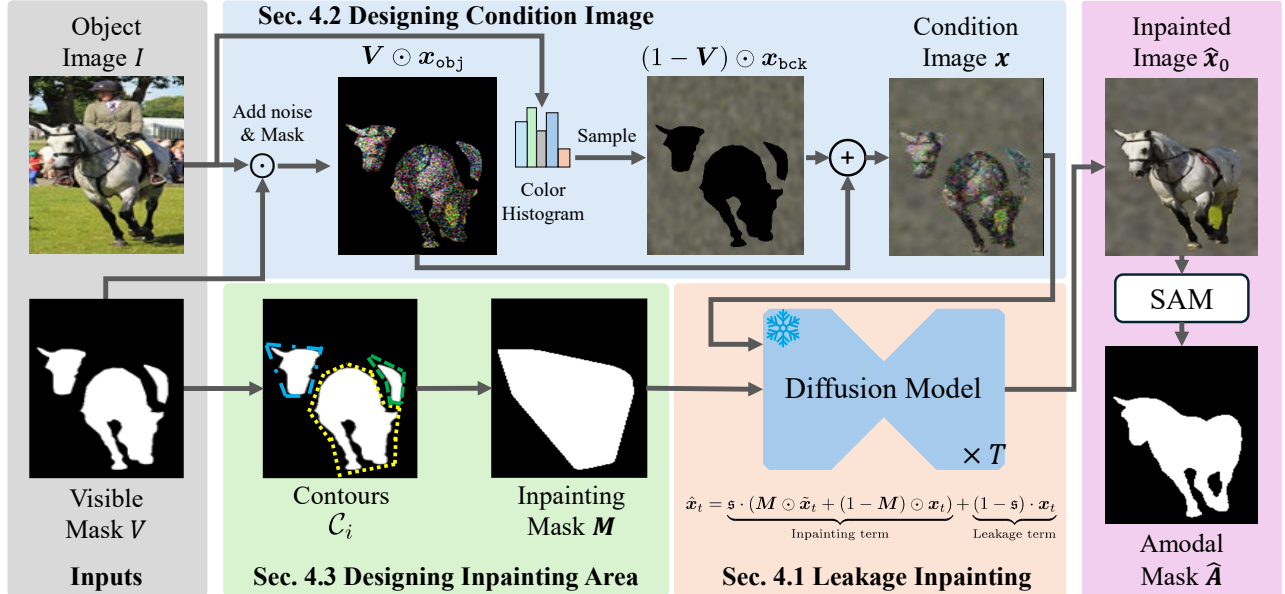


Figure 2. Our approach takes two inputs an RGB image I and a visible mask V . From I , we generate a conditioned RGB image with a color distribution-aware background x_{bck} and a partial Gaussian noise-added object x_{obj} . From V , we create a customized inpainting area M so that we utilize any diffusion-based inpainting models to create an inpainted image \hat{x}_0 to extract amodal mask \hat{A} .

ing as an image denoiser that gradually removes noise according to a schedule. Another common choice, introduced by DDPM [17], is to use a deep-net to model the residual noise ϵ_θ . This is equivalent to choosing a denoiser

$$\mu(x, t) \triangleq x - \sigma_t \cdot \epsilon_\theta(x, t) \quad (3)$$

Inpainting predicts masked-out regions of a given input image. Diffusion-based method [31] leverages the generative prior of a pre-trained DDPM [17] to do so. This is achieved by iteratively removing noise from the linear combination of the noisy unmasked regions with the generated mask regions. More formally, given an input image x and a mask $M \in \{0, 1\}^{H \times W}$ the generation process to produce an inpainted image \hat{x}_0 is as follows:

$$\tilde{x}_t \sim \mathcal{N}(\mu_\theta(\hat{x}_{t-1}, t), \sigma_{t-1}) \quad (4)$$

$$\hat{x}_t = M \odot \tilde{x}_t + (1 - M) \odot x_t \quad (5)$$

where x_t is the noise added input image following Eq. (1), \tilde{x}_T is assumed to be pure noise, and \odot denotes element-wise multiplication. Recent foundation diffusion models [22, 36, 40] are text-conditioned. The denoiser takes in an additional text prompt c to guide the generation, *i.e.*,

$$\tilde{x}_t(c) \sim \mu_\theta(\hat{x}_{t-1}, c, t). \quad (6)$$

4. Training-free Amodal Segmentation

Problem formulation. We consider the amodal segmentation setup as in Ozguroglu et al. [34]. Given an object’s image I and corresponding visible (modal) mask V , the task is to predict the object’s amodal mask \hat{A} that covers the whole object, including occluded regions.

Overview. We propose a tuning-free method for amodal segmentation by re-purposing diffusion inpainting models. Our approach leverages the “occlusion-free” bias of diffusion inpainting models, as shown in Fig. 1, where an inpainted object is almost always generated without occlusion. Hence, we inpaint an occluded object to remove the occlusion and use a segmentation method, *e.g.*, SAM [21], on the unoccluded object to extract the amodal mask \hat{A} . While the proposed method seems straightforward, the devil is in the details.

To achieve high-quality amodal masks, we needed to carefully design the generation procedure of the inpainting model (Sec. 4.1), the conditioning image x (Sec. 4.2), and the inpainting area M (Sec. 4.3). A visual illustration of the approach is provided in Fig. 2.

4.1. Inpainting via leakage conditioning

Recent diffusion inpainting models [22, 36, 40] are often text-conditioned, *i.e.*, the model performs a conditional generation on the masked area with a text-prompt. As the task of amodal segmentation does not involve any text prompt, we need another way to condition the model. Specifically, besides the standard diffusion sampling for inpainting we further “leak” the original unmasked conditioning image x to the model. Instead of Eq. (5), we perform the following:

$$\hat{x}_t = \mathfrak{s} \cdot \underbrace{(M \odot \tilde{x}_t + (1 - M) \odot x_t)}_{\text{Inpainting term}} + \underbrace{(1 - \mathfrak{s}) \cdot x_t}_{\text{Leakage term}}, \quad (7)$$

where $\mathfrak{s} \in \mathbb{R}^+$ controls the strength of the leakage. The purpose of the leakage term is that we want the model to inpaint occluded parts relevant to the current scene context,

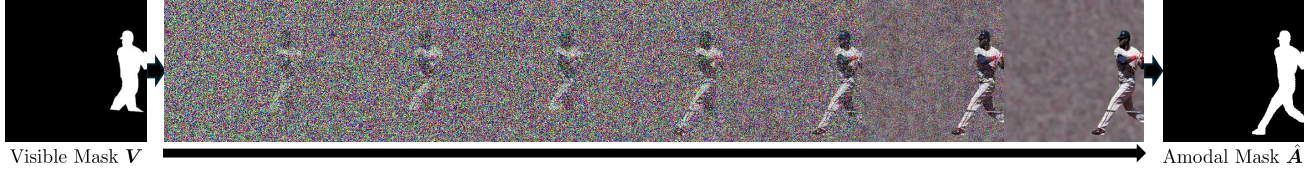


Figure 3. We show a visual process of the diffusion model. As we are doing soft-inpainting, observe that our approach can predict an amodal mask much larger than the visible mask, *i.e.*, extrapolate.

both masked and non-masked regions. Empirically, we set $\varepsilon = 0.3$ to balance the level of image context preservation, which is equivalent to using an image that is the combination of 30% of a newly generated image and 70% of the original image to maintain the overall original context. Increasing noise loses visual contexts, leading to random objects with poor quality of amodal segmentation.

Please note that the update equation in Eq. (7) *no longer strictly* performs image inpainting as the non-masked region is *not* guaranteed to be the same as the conditioning image \mathbf{x} . Instead, we perform a “soft”-inpainting where the model generates an image that roughly resembles the condition image \mathbf{x} for the unmasked regions and focuses on generating within the inpainting area. As the inpainting area is not strict, this also has the benefit that **pixels outside of the inpainting area M can be changed**, *i.e.*, the predicted amodal mask can be larger than the inpainting area M , which helps with cases where extrapolation of the visible mask is needed. To handle this, we leverage the leakage from Eq. (7), which acts like a “soft scaffold”, allowing the model to perform “soft-inpainting”, changing pixels outside the mask. We show this process visually in Fig. 3 and more extrapolation examples in Fig. 7.

4.2. Designing the condition image

The inpainting procedure needs an input condition image, denoted as \mathbf{x} , to guide the generation process. Our objective is to create a complete object without any occlusions. To achieve this, we want the model to focus on the visible parts of the object rather than the background. Therefore, we have a separate procedure for preparing the object and background pixels, where

$$\mathbf{x} = \mathbf{V} \odot \mathbf{x}_{\text{obj}} + (1 - \mathbf{V}) \odot \mathbf{x}_{\text{bck}}. \quad (8)$$

Object pixels. Given the image I containing the object and its corresponding visible mask \mathbf{V} , we extract the object pixels by overlaying the visible mask using an element-wise multiplication. Next, as a diffusion model expected a noisy image, we add noise to the object pixels similar to [4, 33], *i.e.*,

$$\mathbf{x}_{\text{obj}} = (\mathfrak{s} \cdot \epsilon + (1 - \mathfrak{s}) \cdot I), \quad (9)$$

where $\epsilon \sim \mathcal{N}(0, I)$ and $\mathfrak{s} = 0.3$.

Background pixels. In standard inpainting, the pixel values in the masked-out region (background) do not matter. Hence, it is common to choose either black or white color.

However, the background now plays a role due to our leakage conditioning in Eq. (7). The default choice of black or white introduces a sharp contrast around the object’s contours, and diffusion models do not react well to this pixel intensity discontinuity.

Inspired by previous works to blend images seamlessly, such as leveraging the denoising process [31] and incorporating latent information from text-guided diffusion models [2]. We construct a smooth background that matches the object’s color distribution. First, we build a color histogram from the object’s visible pixels in I , then sample background pixels \mathbf{x}_{bck} based on histogram frequencies, and finally apply a Gaussian blur.

4.3. Designing the soft inpainting area

Besides the condition image \mathbf{x} , the inpainting procedure also requires an inpainting area M , which specifies where to focus on the generation.

From the visible mask \mathbf{V} , we extract contours from a set of points corresponding to visible regions, where \mathcal{C}_i is the i^{th} contour. Next, we combine the contours into one region by taking their union and finding the smallest convex polygon $\text{ConvHull}(\bigcup_{i=1} \mathcal{C}_i)$ that can enclose all contours. Finally, we get the inpainting region, M , by setting values inside the convex polygon to one, where a visible pixel at (x, y) :

$$M = \begin{cases} 1, & \text{if } (x, y) \in \text{ConvHull}(\bigcup_{i=1} \mathcal{C}_i), \\ 0, & \text{otherwise.} \end{cases} \quad (10)$$

Next, diffusion inpainting models are trained to take an inpainting region as conditioning input, *i.e.*, $\tilde{\mathbf{x}}_t(M)$. Hence, this allows us to use classifier-free guidance [16] with the mask during the generation. Let w denote the intensity of the strictness which is how the model needs to follow the conditioning of the inpainting region M a classifier-free-guided sample computes

$$\tilde{\mathbf{x}}_t^{\text{CFG}} = (1 + w) \cdot \tilde{\mathbf{x}}_t(M) - w \cdot \tilde{\mathbf{x}}_t(\emptyset), \quad (11)$$

where \emptyset denotes the empty representation of M . Instead of using $\tilde{\mathbf{x}}$ directly in Eq. (5), $\tilde{\mathbf{x}}_t^{\text{CFG}}$ is used. Intuitively, smaller w gives more freedom to generate new pixel information independent of the inpainting area shape. Empirically, we set $w = 0.75$ for Stable Diffusion version 1.5 [40], Stable Diffusion XL [36] and w as 1.5 with Flux [22].

Method	DiffMod	COCO	BSDS	KINS	FBowl	SV	Avg
pix2gestalt	SD2	82.9	80.8	39.2	73.3	52.3	65.7
Amodal Wild	-	90.2	-	-	-	-	-
SAM	-	66.6	65.3	40.8	68.3	55.9	59.4
SAM2	-	70.1	63.1	46.9	65.5	57.0	60.5
Inpaint	SDXL	76.5	74.2	-	-	-	-
Ours	SDXL	82.7	75.6	60.4	73.0	63.5	71.0
Ours	SD1.5	79.9	75.2	58.4	71.0	66.6	70.2
Ours	SD2	73.2	72.6	57.2	72.8	57.2	66.6
Ours	Flux	75.5	75.5	60.2	75.2	65.6	70.4

Table 1. Quantitative comparisons of amodal mask in mIoU(%) \uparrow . Methods except for pix2gestalt are tuning-free. The best result is bolded, and the second best is colored in blue.

5. Experiments

Our method is tuning-free, and also a zero-shot amodal segmentation method. For a fair comparison, we strictly follow the experiment setup of zero-shot amodal segmentation experiment setting by Ozguroglu et al. [34] on COCO-A [62] and BSDS-A [61]. To study the zero-shot capability, we evaluate three additional datasets, including KINS [37], FishBowl [45], and SAILVOS [18]. We report quantitative and qualitative results followed by ablations.

5.1. Experiment setup

We report on the following five datasets covering both real-world and synthetic images:

- 1 COCO-A [62]: Based on COCO [27] dataset, COCO-A [62] is a human-annotated amodal segmentation dataset over natural images. We report on its evaluation set with 13k ground truth object amodal annotations in 2.5k images, including common objects.
- 2 BSDS-A [61]: Derived from the Berkeley Segmentation Dataset (BSDS) [32], BSDS-A [61] is an amodal segmentation dataset labeled with manual amodal annotation. We report on the evaluation image sets with 200 images from the real world.
- 3 KINS [37]: KINS [37], derived from KITTI [12] for autonomous driving, features manually annotated amodal masks and an evaluation set of 7k images.
- 4 FishBowl (Fbowl) [45] is a synthetic dataset that has different numbers of fish from an WebGL demo [48]. Its evaluation set contains 1k videos of 128 frames each, with each frame treated independently for amodal segmentation.
- 5 SAILVOS (SV) [18] is a synthetic dataset from the photo-realistic game GTA-V. It contains 26k images along with 507k objects in the evaluation set.

Evaluation metric. Following Ozguroglu et al. [34], we report the mean intersection over union (mIoU) to evaluate predicted amodal masks. A higher mIoU indicates a better match of the prediction with the ground truth. We also report the mIoU over different subsets of the data based on the occlusion rate of the object. Specifically, we report on oc-

Method	DiffMod	$\leq 50\%$	$\leq 40\%$	$\leq 30\%$	$\leq 20\%$	$\leq 10\%$	$\leq 5\%$
pix2gestalt	SD2	83.1	83.7	84.3	85.2	86.7	87.0
Amodal Wild	-	86.7	88.3	88.6	89.9	93.3	92.2
SAM	-	68.4	71.2	73.7	76.3	79.9	81.2
SAM2	-	70.0	72.8	75.6	78.5	81.9	83.4
Ours	SD1.5	79.9	82.9	85.9	88.8	92.1	93.6
Ours	SDXL	82.7	85.4	88.0	90.6	93.6	95.0
Ours	SD2	77.5	79.8	82.1	84.1	87.1	88.3
Ours	Flux	76.2	77.2	78.7	80.4	83.2	84.1

Table 2. We compare the quality of amodal mask in mIoU(%) \uparrow from COCO-A [62].

clusion rate subsets that are less than 50%. We observed that highly occluded objects yield uncertain annotations, as images often lack enough details for a complete amodal mask.

Baselines. We consider the state-of-the-art baseline of pix2gestalt, two training-required methods, and three additional tuning-free methods.

- 1 pix2gestalt [34] takes an RGB image and its modal mask to generate an amodal mask by using SAM [21] to collect on a customized training dataset that has more than 800k image pairs with occlusions to a fine-tuned a *pre-trained diffusion model* of StableDiffusion2 (SD2) [43].
- 2 Amodal Wild [59] uses a two-stage approach. First, an occluder mask is predicted from an RGB image and its modal mask. Next, a U-Net-based model leveraging features from a pre-trained Stable Diffusion (using the modal mask and occluder boundary) predicts the amodal mask.
- 3 Inpaint-SDXL [36]: Given a visible mask and an RGB image, SDXL inpaints its region by leveraging a pre-trained model to remove missing pixel information. This baseline is proposed by Ozguroglu et al. [34] in pix2gestalt. We directly report the number from their paper, as the code for this baseline has not been released.
- 4 SAM [21]: takes a set of points and an RGB image to segment pixels that fall into the same object category based on features from an image encoder. This is a strong modal baseline, as reported by Ozguroglu et al. [34]
- 5 SAM2 [39]: We also consider a even strong modal baseline of SAM2, which is a improved version of SAM.

We also tried comparing to Amodal Completion by Xu et al. [50], however, as it is limited to 83 categories, the approach was unable to generate a prediction for many images in the datasets we considered.

Implementation. We consider several popular diffusion models, including Stable Diffusion 1.5 and 2 (SD1.5, SD2) [40], Stable Diffusion XL (SDXL) [36], and Flux [22]. We set $\epsilon = 0.3$, $w = 7.5$ for Stable Diffusion 1.5 [40] and Stable Diffusion XL [36], and $w = 1.5$ for Flux [22]. Images are refined with 20 iterative steps for amodal completion, and the mask M is extracted by uniformly sampling nine points from V using SAM [21]. All experiments were performed on an NVIDIA RTX 4090 (24GB VRAM), and 8-bit quantization was applied for Flux to reduce the memory usage.

Method	DiffMod	$\leq 50\%$	$\leq 40\%$	$\leq 30\%$	$\leq 20\%$	$\leq 10\%$	$\leq 5\%$
pix2gestalt	SD2	77.1	78.0	79.0	80.2	81.4	81.9
SAM	-	62.1	64.6	66.8	69.3	72.6	74.9
SAM2	-	63.4	66.6	69.4	72.4	76.7	78.6
Ours	SD1.5	78.3	80.5	82.5	84.5	86.7	87.4
Ours	SDXL	75.7	79.2	82.2	85.7	88.9	90.7
Ours	SD2	76.2	79.8	82.8	85.8	88.7	90.1
Ours	Flux	76.4	78.5	81.0	84.1	85.9	72.6

Table 3. We compare the quality of amodal mask in mIoU(%) \uparrow from BSDS-A [61].

Method	DiffMod	$\leq 50\%$	$\leq 40\%$	$\leq 30\%$	$\leq 20\%$	$\leq 10\%$	$\leq 5\%$
pix2gestalt	SD2	39.1	40.2	41.7	43.7	48.0	55.1
SAM	-	42.2	42.8	43.7	44.8	47.3	50.8
SAM2	-	48.7	49.6	50.7	52.3	54.9	58.3
Ours	SD1.5	64.8	66.2	68.2	70.6	74.1	77.3
Ours	SDXL	60.4	62.1	64.1	66.6	70.8	75.1
Ours	SD2	60.2	61.4	63.0	64.8	68.1	73.5
Ours	Flux	64.7	65.4	67.3	69.5	72.7	75.6

Table 4. We compare the quality of amodal mask in mIoU(%) \uparrow from KINS [37].

5.2. Quantitative results

Main results. Tab. 1 reports mIoU using five datasets, and we **bold** the best metric and **colored** the second best metric. For the COCO-A [62] and BSDS-A [61], pix2gestalt [34] (a non-tuning free method) has the best metrics, followed by Stable Diffusion XL with ours by 0.2% and 5.2%.

We highlight that the first two datasets are reported in pix2gestalt to study zero-shot amodal segmentation. Recall that their approach trains on a “synthetically curated dataset” and is hence zero-shot. However, it is unclear whether this curated dataset generalizes beyond COCO-A and BSDS-A *e.g.*, what if the testing distribution is very different from their curated data.

We report on three additional datasets with various object categories to further study the zero-shot capability. On KINS [37], FishBowl (FBowl) [45], SAILVOS (SV) [18], show that our methods generate 21.2%, 1.9%, and 14.3% more accurate mask than pix2gestalt. Importantly, our method performs best from the tuning-free approaches and convincingly outperforms the modal baseline. We could not compare on inpainting-SDXL, as the code was not released, and we could not reproduce it.

Below, we report and discuss the detailed results based on different object occlusion rates. In the appendix, we provide further qualitative analysis for each dataset.

Detailed COCO-A results. Tab. 2 shows the performance based on our approach using four foundation models (Stable Diffusion 1.5 [40], Stable Diffusion XL [36], Stable Diffusion 2 [43], Flux [22]) to pix2gestalt [34] along with SAM [21] and SAM2 [39].

Our work using Stable Diffusion XL [36] generates 1.7%, 3.7%, 5.4%, 6.9%, and 8.0% more accurate amodal

Method	DiffMod	$\leq 50\%$	$\leq 40\%$	$\leq 30\%$	$\leq 20\%$	$\leq 10\%$	$\leq 5\%$
pix2gestalt	SD2	77.1	78.0	79.0	80.2	81.4	81.9
SAM	-	60.9	63.0	65.0	67.3	70.4	74.3
SAM2	-	68.0	69.8	72.4	74.4	77.1	79.8
Ours	SD1.5	79.0	81.3	83.8	86.7	89.6	90.1
Ours	SDXL	79.5	81.1	83.6	85.3	87.1	87.5
Ours	SD2	77.9	79.3	80.7	81.9	82.7	82.9
Ours	Flux	80.4	82.8	85.3	88.0	90.7	91.9

Table 5. We compare the quality of amodal mask in mIoU(%) \uparrow from FishBowl [45].

Method	DiffMod	$\leq 50\%$	$\leq 40\%$	$\leq 30\%$	$\leq 20\%$	$\leq 10\%$	$\leq 5\%$
pix2gestalt	SD2	59.4	60.2	61.3	62.9	65.6	67.8
SAM	-	66.2	68.7	71.1	73.5	76.2	79.3
SAM2	-	67.5	69.9	72.2	74.5	76.8	79.2
Ours	SD1.5	80.0	82.3	84.1	85.8	87.4	88.7
Ours	SDXL	62.3	64.0	65.7	67.5	70.5	72.1
Ours	SD2	68.6	70.1	71.6	73.2	75.9	77.7
Ours	Flux	79.3	81.8	83.6	85.4	87.2	88.8

Table 6. We compare the quality of amodal mask in mIoU(%) \uparrow from SAILVOS.

masks on average when objects are occluded less than equal to 40%, 30%, 20%, 10%, and 5% compared to pix2gestalt, respectively and it has a 0.2% higher mIoU as shown Tab. 1.

While the training-required method [59] achieves a 7% mIoU gain, our approach improves 0.7%, 0.3%, and 2.8% at 20%, 10%, and 5% occlusion, respectively.

Detailed BSDS-A results. In Tab. 3, our method has higher 1.2% and 2.5% mIoU with Stable Diffusion 1.5 [40] at 50% and 40% occlusion, 3.8% and 5.6% with Stable Diffusion 2 [43] at 30% and 20%, and 5.9% and 6.6% with Stable Diffusion XL [36] at 10% and 5%, compared to pix2gestalt [34]. Our method achieves 4.9% more accurate amodal mask on average for occlusions under 50%.

Detailed KINS results. In Tab. 4, Stable Diffusion 1.5 [40] with our approach predicts 25.7%, 26%, 26.5%, 26.9%, 26.1%, and 22.2% more accurate amodal masks, in all occlusion rates, compared to pix2gestalt [34]. On average, our method outperforms 25.6% to generate an accurate amodal mask with occlusion rates of 50% or less. The largest performance gap among the five datasets comes from pix2gestalt’s training data, which is insufficient to cover KINS [37] occlusions, leading to robustness issues.

Detailed FishBowl results. In Tab. 5, our approach with Flux [22] shows 1.2%, 3.3%, 5.7%, 8.4%, and 9.6% more accurate amodal mask than pix2gestalt [34]. For occlusion rates of 50% or less, our method predicts an average mIoU that is 6.9% higher than pix2gestalt, further demonstrating the zero-shot capabilities.

Detailed SAILVOS results. Tab. 6 shows that our approach generates 20.6%, 22.1%, 22.8%, 22.9%, 21.8%, 21% more precise amodal mask than pix2gestalt [34], averaging 21.9% higher mIoU for occlusions $\leq 50\%$.

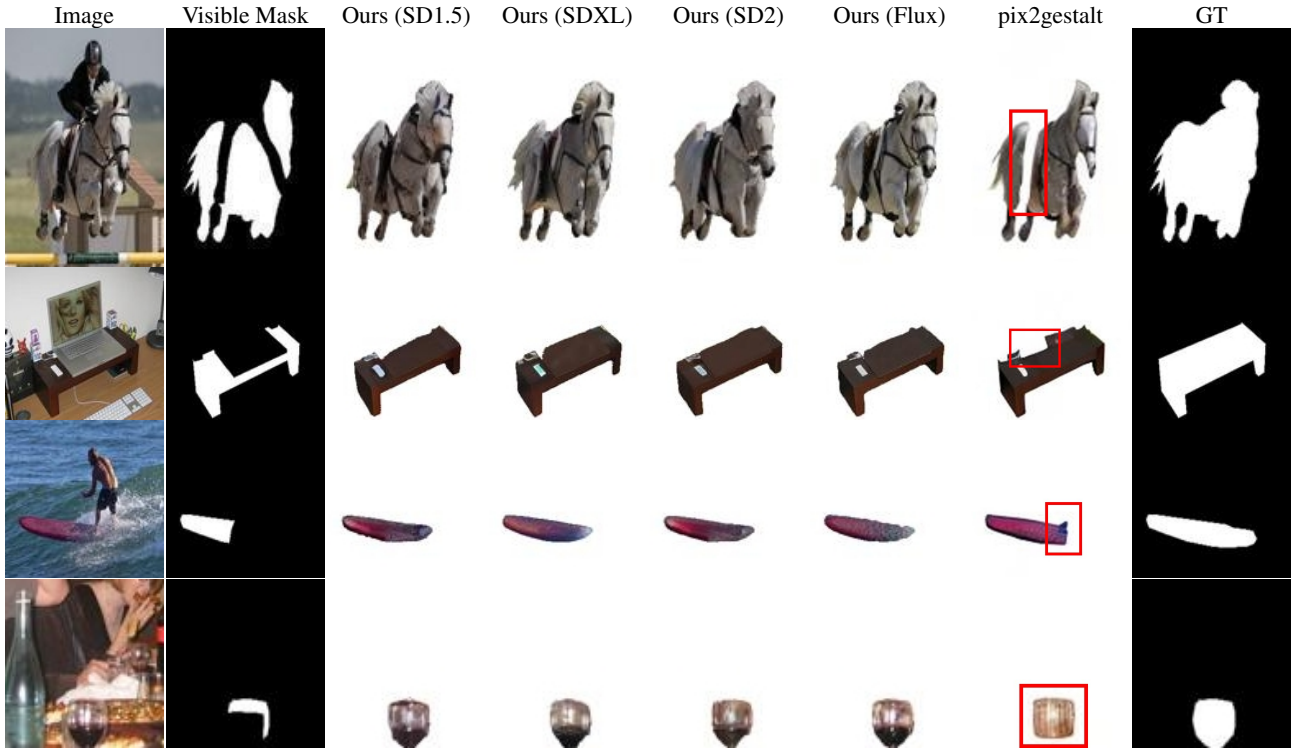


Figure 4. We compare the accuracy of amodal mask in COCO-A [62] and BSDS-A [61] using various diffusion-based inpainting models. Keep in mind that we focus on generating accurate amodal masks rather than on synthesizing an accurate and high-quality image. We highlight incomplete and out-of-shape areas using a red box.

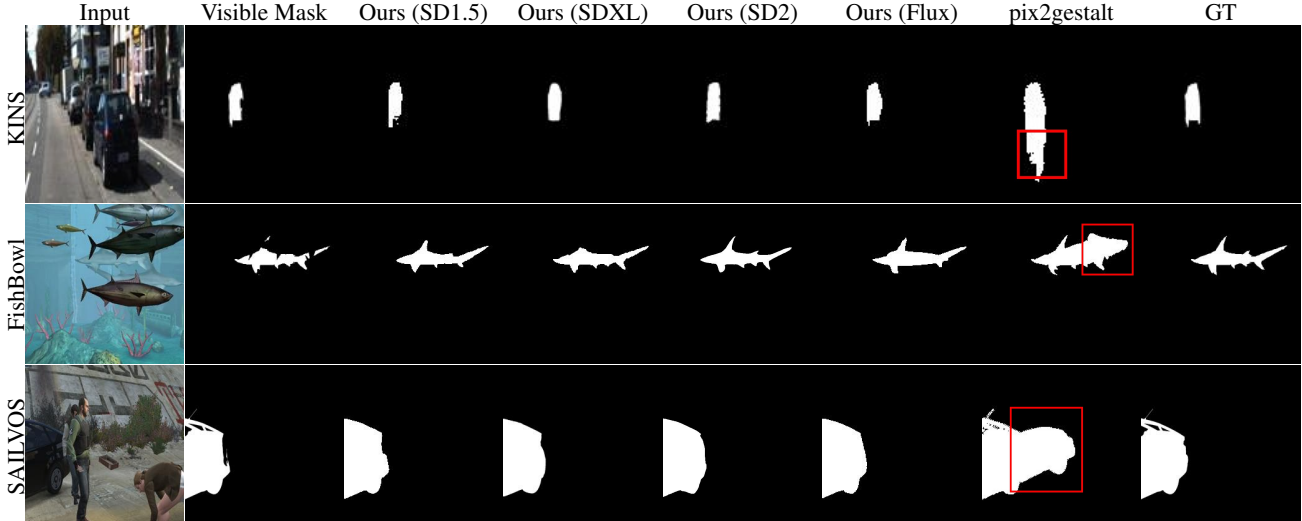


Figure 5. Qualitative comparison of amodal mask on KINS [37], FishBowl [45], and SAILVOS [18]. We observe that for novel categories/ domain pix2gestalt may hallucinate inaccurate amodal masks.

5.3. Qualitative results

We compare the visual quality of the amodal mask in Fig. 4. Please remember that our goal is not to generate high-quality inpainted results. That is, one should judge how closely the contour of the inpainted object matches the ground truth. Our method successfully predicts the oc-

cluded regions, *e.g.*, removing the occlusion and generating a complete horse. On the other hand, pix2gestalt fails to generate in the occluded areas (rows 1 and 2) and struggles to handle the outside of the visible area (rows 3 and 4).

Next, we further show the amodal mask generation results on the three additional datasets, including KINS [37]



Figure 6. Amodal completion results on in-the-wild images comparing Ours (SDXL) and pix2gestalt [34].

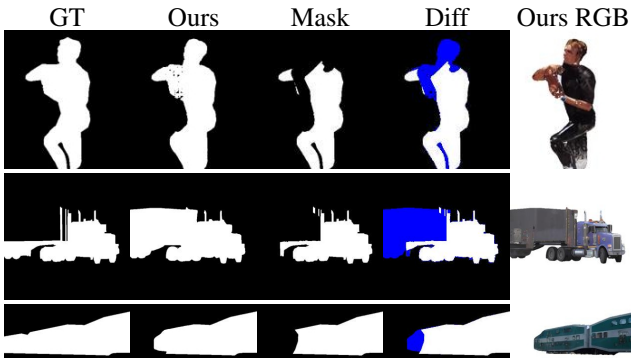


Figure 7. Blue pixels denote differences between the visible mask and our predicted mask.

(row 1), FishBowl [45] (row 2), and SAILVOS [18] (row 3) in Fig. 5. The first row shows that pix2gestalt overextends the car. The second row demonstrates that pix2gestalt misunderstands the visual context and adds “hallucinations”, which is another car, to generate amodal masks. Overall, we observe that pix2gestalt performs worse on these additional datasets, possibly due to a larger gap in distribution from their curated data. In contrast, our method shows robustness with high-quality amodal masks.

We also experimented with in-the-wild images to validate our approaches compared to pix2gestalt (Fig. 6). We start with the horse (first row) that pix2gestalt reported in their paper. The predicted mask from our approach shows a comparable quality to that generated by pix2gestalt. We also show another example (second row), where ours completes a cloth behind the cup that Grogu is holding, while pix2gestalt barely made any changes to the input image. Moreover, Fig. 7 shows cases of amodal mask extrapolation, demonstrating our method’s robustness.

5.4. Ablation studies & analysis

Ablations. We evaluate the effectiveness of each component by removing them in Tab. 7. The experiment is conducted on COCO-A [62] using Stable Diffusion XL [36]. The first row shows the mIoU with all the components

DiffMod	Leakage	Background	Mask	mIoU(%) \uparrow
SDXL	✓	✓	✓	76.5
SDXL	✗	✓	✓	38.9
SDXL	✓	✗	✓	70.9
SDXL	✓	✓	✗	70.3

Table 7. We show our component’s effectiveness using mIoU by excluding each component from the pipeline.

ε	$\leq 50\%$	$\leq 40\%$	$\leq 30\%$	$\leq 20\%$	$\leq 10\%$	$\leq 5\%$
0.1	75.0	77.5	80.1	82.5	86.3	87.9
0.15	75.8	78.2	80.7	83.0	86.6	88.1
0.3	79.9	82.9	85.9	88.8	92.1	93.6
0.45	75.1	77.2	79.2	81.2	84.4	85.5
0.6	69.6	71.3	73.1	75.1	78.5	79.4
0.9	60.1	61.6	63.0	64.4	66.1	67.1

Table 8. The impact of ε using mIoU(%) from COCO-A.

M -type	background	$\leq 50\%$	$\leq 40\%$	$\leq 30\%$	$\leq 20\%$	$\leq 10\%$	$\leq 5\%$
Ours	Ours	79.9	82.9	85.9	88.8	92.1	93.6
Rect.	Ours	77.7	80.0	82.1	84.1	86.9	88.2
Ours	White	71.4	73.8	76.2	78.6	81.8	83.1
Rect.	White	70.3	72.9	75.2	77.7	81.0	82.3

Table 9. Comparisons with a different mask and color histogram.

included. When the leaking conditioning (Sec. 4.1), the context-aware background (Sec. 4.2), or the inpainting area (Sec. 4.3) is excluded, the accuracy of the amodal mask falls by 37.6%, 5.6%, 6.2% in the mIoU compared to using all components respectively and the greater drop indicates higher importance for generating accurate amodal masks. Moreover, we ablate the value of ε (Tab. 8). In Tab. 9, we verify the effectiveness of our designed inpainting region, M , along with the context-aware background by comparing it to a simple rectangular mask with a white background.

Computation efficiency. We compare the efficiency of our approach to pix2gestalt. For the smallest model, SD2 is $4.1\times$ more efficient in memory, and the inference (0.3 seconds) is $19\times$ faster compared to pix2gestalt [34]. Additionally, our best model (SDXL) is also more efficient than pix2gestalt. See Tab. S1 in the Appendix for more results.

6. Conclusion

We introduce a tuning-free/zero-shot amodal segmentation method by leveraging the occlusion-fere bias of pre-trained diffusion inpainting models. Our approach customizes the conditioning image, designs a new inpainting region, and uses a novel leakage conditioning technique. Experiments on five datasets demonstrate that our model (SDXL) improves mIoU by **5.3%**, with **4.8** \times faster inference and **1.4** \times VRAM efficiency over pix2gestalt. Other models (SD1.5, SD2, Flux) are also effective. As diffusion inpainting techniques continue to improve, we anticipate further advancements in segmentation performance.

References

- [1] Jiayang Ao, Qihong Ke, and Krista A Ehinger. Amodal intra-class instance segmentation: Synthetic datasets and benchmark. In *WACV*, 2024. 1
- [2] Omri Avrahami, Dani Lischinski, and Ohad Fried. Blended diffusion for text-driven editing of natural images. In *CVPR*, 2022. 4
- [3] Mathilde Caron, Hugo Touvron, Ishan Misra, Hervé Jégou, Julien Mairal, Piotr Bojanowski, and Armand Joulin. Emerging properties in self-supervised vision transformers. In *ICCV*, 2021. 1
- [4] Ciprian Corneanu, Raghudeep Gadde, and Aleix M Martinez. Latentpaint: Image inpainting in latent space with diffusion models. In *WACV*, 2024. 2, 4
- [5] Tung Dang, Frank Mascariach, Shehryar Khattak, Christos Papachristos, and Kostas Alexis. Graph-based path planning for autonomous robotic exploration in subterranean environments. In *IEEE/RSJ IROS*, 2019. 1
- [6] Soheil Darabi, Eli Shechtman, Connelly Barnes, Dan B Goldman, and Pradeep Sen. Image melding: Combining inconsistent images using patch-based synthesis. *ACM TOG*, 2012. 2
- [7] Gangui Ding, Canyu Zhao, Wen Wang, Zhen Yang, Zide Liu, Hao Chen, and Chunhua Shen. Freecustom: Tuning-free customized image generation for multi-concept composition. In *CVPR*, 2024. 2
- [8] Kiana Ehsani, Roozbeh Mottaghi, and Ali Farhadi. Segan: Segmenting and generating the invisible. In *CVPR*, 2018. 2
- [9] Hao Fei, Shengqiong Wu, Wei Ji, Hanwang Zhang, and Tat-Seng Chua. Dysen-vdm: Empowering dynamics-aware text-to-video diffusion with llms. In *CVPR*, 2024. 3
- [10] Patrick Follmann, Rebecca König, Philipp Härtinger, Michael Klostermann, and Tobias Böttger. Learning to see the invisible: End-to-end trainable amodal instance segmentation. In *WACV*, 2019. 1
- [11] Jianxiong Gao, Xuelin Qian, Yikai Wang, Tianjun Xiao, Tong He, Zheng Zhang, and Yanwei Fu. Coarse-to-fine amodal segmentation with shape prior. In *ICCV*, 2023. 2
- [12] Andreas Geiger, Philip Lenz, and Raquel Urtasun. Are we ready for autonomous driving? the kitti vision benchmark suite. In *CVPR*, 2012. 1, 5
- [13] Qiang Guo, Shanshan Gao, Xiaofeng Zhang, Yilong Yin, and Caiming Zhang. Patch-based image inpainting via two-stage low rank approximation. *IEEE TVCG*, 2017. 2
- [14] Xiefan Guo, Hongyu Yang, and Di Huang. Image inpainting via conditional texture and structure dual generation. In *ICCV*, 2021. 2
- [15] Yingqing He, Shaoshu Yang, Haoxin Chen, Xiaodong Cun, Menghan Xia, Yong Zhang, Xintao Wang, Ran He, Qifeng Chen, and Ying Shan. Scalecrafter: Tuning-free higher-resolution visual generation with diffusion models. In *ICLR*, 2023. 2
- [16] Jonathan Ho and Tim Salimans. Classifier-free diffusion guidance. *arXiv preprint arXiv:2207.12598*, 2022. 4
- [17] Jonathan Ho, Ajay Jain, and Pieter Abbeel. Denoising diffusion probabilistic models. *NeurIPS*, 2020. 2, 3
- [18] Y.-T. Hu, H.-S. Chen, K. Hui, J.-B. Huang, and A. G. Schwing. SAIL-VOS: Semantic Amodal Instance Level Video Object Segmentation – A Synthetic Dataset and Baselines. In *CVPR*, 2019. 1, 2, 5, 6, 7, 8, 3
- [19] Kyong Hwan Jin and Jong Chul Ye. Annihilating filter-based low-rank hankel matrix approach for image inpainting. *IEEE TIP*, 2015. 2
- [20] K8xu. Official code of amodal completion via progressive mixed context diffusion. <https://github.com/k8xu/amodal/blob/main/classes.txt>, 2025. 2
- [21] Alexander Kirillov, Eric Mintun, Nikhila Ravi, Hanzi Mao, Chloe Rolland, Laura Gustafson, Tete Xiao, Spencer Whitehead, Alexander C Berg, Wan-Yen Lo, et al. Segment anything. In *ICCV*, 2023. 1, 3, 5, 6
- [22] Black Forest Labs. FLUX.1 [Schnell]. <https://huggingface.co/black-forest-labs/FLUX.1-schnell>, 2024. [Accessed 09-09-2024]. 3, 4, 5, 6, 1, 2
- [23] Steven Lehar. Gestalt isomorphism and the quantification of spatial perception. *Gestalt theory*, 1999. 2
- [24] Jingyuan Li, Ning Wang, Lefei Zhang, Bo Du, and Dacheng Tao. Recurrent feature reasoning for image inpainting. In *CVPR*, 2020. 2
- [25] Ke Li and Jitendra Malik. Amodal instance segmentation. In *ECCV*, 2016. 1, 2
- [26] Wenbo Li, Zhe Lin, Kun Zhou, Lu Qi, Yi Wang, and Jiaya Jia. Mat: Mask-aware transformer for large hole image inpainting. In *CVPR*, 2022. 2
- [27] Tsung-Yi Lin, Michael Maire, Serge Belongie, James Hays, Pietro Perona, Deva Ramanan, Piotr Dollár, and C Lawrence Zitnick. Microsoft coco: Common objects in context. In *ECCV*, 2014. 5
- [28] Guilin Liu, Aysegul Dundar, Kevin J Shih, Ting-Chun Wang, Fitsum A Reda, Karan Sapra, Zhiding Yu, Xiaodong Yang, Andrew Tao, and Bryan Catanzaro. Partial convolution for padding, inpainting, and image synthesis. *IEEE TPAMI*, 2022. 2
- [29] Kendong Liu, Zhiyu Zhu, Chuanhao Li, Hui Liu, Huanqiang Zeng, and Junhui Hou. Prepaint: Aligning image inpainting diffusion model with human preference. *arXiv preprint arXiv:2410.21966*, 2024. 2
- [30] Jonathan Long, Evan Shelhamer, and Trevor Darrell. Fully convolutional networks for semantic segmentation. In *CVPR*, 2015. 1
- [31] Andreas Lugmayr, Martin Danelljan, Andres Romero, Fisher Yu, Radu Timofte, and Luc Van Gool. Repaint: Inpainting using denoising diffusion probabilistic models. In *CVPR*, 2022. 2, 3, 4
- [32] D. Martin, C. Fowlkes, D. Tal, and J. Malik. A database of human segmented natural images and its application to evaluating segmentation algorithms and measuring ecological statistics. In *ICCV*, 2001. 5
- [33] Chenlin Meng, Yutong He, Yang Song, Jiaming Song, Jiajun Wu, Jun-Yan Zhu, and Stefano Ermon. SDEdit: Guided image synthesis and editing with stochastic differential equations. In *ICLR*, 2022. 4

- [34] Ege Ozguroglu, Ruoshi Liu, Dídac Surés, Dian Chen, Achal Dave, Pavel Tokmakov, and Carl Vondrick. pix2gestalt: Amodal segmentation by synthesizing wholes. *CVPR*, 2024. 1, 2, 3, 5, 6, 8
- [35] William Peebles and Saining Xie. Scalable diffusion models with transformers. In *ICCV*, 2023. 1
- [36] Dustin Podell, Zion English, Kyle Lacey, Andreas Blattmann, Tim Dockhorn, Jonas Müller, Joe Penna, and Robin Rombach. Sdxl: Improving latent diffusion models for high-resolution image synthesis. *arXiv preprint arXiv:2307.01952*, 2023. 1, 3, 4, 5, 6, 8, 2
- [37] Lu Qi, Li Jiang, Shu Liu, Xiaoyong Shen, and Jiaya Jia. Amodal instance segmentation with kins dataset. In *CVPR*, 2019. 2, 5, 6, 7, 1, 3
- [38] Haonan Qiu, Menghan Xia, Yong Zhang, Yingqing He, Xintao Wang, Ying Shan, and Ziwei Liu. Freenoise: Tuning-free longer video diffusion via noise rescheduling. In *ICLR*, 2024. 2
- [39] Nikhila Ravi, Valentin Gabeur, Yuan-Ting Hu, Ronghang Hu, Chaitanya Ryali, Tengyu Ma, Haitham Khedr, Roman Rädle, Chloe Rolland, Laura Gustafson, Eric Mintun, Junting Pan, Kalyan Vasudev Alwala, Nicolas Carion, Chaoyuan Wu, Ross Girshick, Piotr Dollár, and Christoph Feichtenhofer. SAM2: Segment anything in images and videos. *arXiv preprint arXiv:2408.00714*, 2024. 5, 6
- [40] Robin Rombach, Andreas Blattmann, Dominik Lorenz, Patrick Esser, and Björn Ommer. High-resolution image synthesis with latent diffusion models. In *CVPR*, 2022. 1, 2, 3, 4, 5, 6
- [41] Olaf Ronneberger, Philipp Fischer, and Thomas Brox. U-net: Convolutional networks for biomedical image segmentation. In *MICCAI*, 2015. 1
- [42] Chitwan Saharia, William Chan, Huiwen Chang, Chris Lee, Jonathan Ho, Tim Salimans, David Fleet, and Mohammad Norouzi. Palette: Image-to-image diffusion models. In *ACM SIGGRAPH*, 2022. 2
- [43] Stability-AI. Stability-ai/stablediffusion: High-resolution image synthesis with latent diffusion models. <https://github.com/Stability-AI/stablediffusion>, 2024. [Accessed 11-04-2024]. 5, 6, 1, 2, 3
- [44] Roman Suvorov, Elizaveta Logacheva, Anton Mashikhin, Anastasia Remizova, Arsenii Ashukha, Aleksei Silvestrov, Naejin Kong, Harshith Goka, Kiwoong Park, and Victor Lempitsky. Resolution-robust large mask inpainting with fourier convolutions. In *WACV*, 2022. 2
- [45] Matthias Tangemann, Steffen Schneider, Julius Von Kügelgen, Francesco Locatello, Peter Gehler, Thomas Brox, Matthias Kümmerer, Matthias Bethge, and Bernhard Schölkopf. Unsupervised object learning via common fate. *arXiv preprint arXiv:2110.06562*, 2021. 2, 5, 6, 7, 8, 1, 3
- [46] Minh Tran, Khoa Vo, Kashu Yamazaki, Arthur Fernandes, Michael Kidd, and Ngan Le. Aisformer: Amodal instance segmentation with transformer. *arXiv preprint arXiv:2210.06323*, 2022. 2
- [47] David Tschumperlé and Rachid Deriche. Vector-valued image regularization with pdes: A common framework for different applications. *IEEE TPAMI*, 2005. 2
- [48] WebGLSamples. WebGL Aquarium — webglsamples.org. <https://webglsamples.org/aquarium/aquarium.html>, 2024. [Accessed 16-09-2024]. 5
- [49] Yuting Xiao, Yanyu Xu, Ziming Zhong, Weixin Luo, Jiawei Li, and Shenghua Gao. Amodal segmentation based on visible region segmentation and shape prior. In *AAAI*, 2021. 1, 2
- [50] Katherine Xu, Lingzhi Zhang, and Jianbo Shi. Amodal completion via progressive mixed context diffusion. In *CVPR*, 2024. 1, 2, 5
- [51] Jianwei Yang, Zhile Ren, Mingze Xu, Xinlei Chen, David J Crandall, Devi Parikh, and Dhruv Batra. Embodied amodal recognition: Learning to move to perceive objects. In *ICCV*, 2019. 1, 2
- [52] Lihe Yang, Bingyi Kang, Zilong Huang, Xiaogang Xu, Jiashi Feng, and Hengshuang Zhao. Depth anything: Unleashing the power of large-scale unlabeled data. In *CVPR*, 2024. 2
- [53] Raymond A Yeh, Chen Chen, Teck Yian Lim, Alexander G Schwing, Mark Hasegawa-Johnson, and Minh N Do. Semantic image inpainting with deep generative models. In *CVPR*, 2017. 2
- [54] Ahmet Burak Yildirim, Hamza Pehlivan, Bahri Batuhan Bilecen, and Aysegul Dunder. Diverse inpainting and editing with gan inversion. In *ICCV*, 2023.
- [55] Jiahui Yu, Zhe Lin, Jimei Yang, Xiaohui Shen, Xin Lu, and Thomas S Huang. Free-form image inpainting with gated convolution. In *ICCV*, 2019. 2
- [56] Alan Yuille and Daniel Kersten. Vision as bayesian inference: analysis by synthesis? *Trends in cognitive sciences*, 2006. 2
- [57] Yu Zeng, Zhe Lin, Jimei Yang, Jianming Zhang, Eli Shechtman, and Huchuan Lu. High-resolution image inpainting with iterative confidence feedback and guided upsampling. In *ECCV*, 2020. 2
- [58] Yu Zeng, Vishal M Patel, Haochen Wang, Xun Huang, Ting-Chun Wang, Ming-Yu Liu, and Yogesh Balaji. Jedi: Joint-image diffusion models for finetuning-free personalized text-to-image generation. In *CVPR*, 2024. 2
- [59] Guanqi Zhan, Chuanxia Zheng, Weidi Xie, and Andrew Zisserman. Amodal ground truth and completion in the wild. In *CVPR*, 2024. 2, 5, 6
- [60] Ziheng Zhang, Anpei Chen, Ling Xie, Jingyi Yu, and Shenghua Gao. Learning semantics-aware distance map with semantics layering network for amodal instance segmentation. In *ACM MM*, 2019. 2
- [61] Yan Zhu, Yuandong Tian, Dimitris Metaxas, and Piotr Dollár. Semantic amodal segmentation. In *CVPR*, 2017. 2, 5, 6, 7, 1, 3
- [62] Yan Zhu, Yuandong Tian, Dimitris Metaxas, and Piotr Dollár. Semantic amodal segmentation. In *CVPR*, 2017. 2, 5, 6, 7, 8, 1, 3

Tuning-Free Amodal Segmentation via the Occlusion-Free Bias of Inpainting Models

Supplementary Material

The appendix is organized as follows:

- In Sec. S1, we provide additional qualitative results.
- In Sec. S2, we conduct additional ablations by comparing two different ways of creating mask regions.
- In Sec. S3, we provide implementation details.

S1. Additional Qualitative Analysis

We demonstrate a more detailed qualitative analysis using the four foundation diffusion-based inpainting models, SD1.5 [40], SD2 [43], SDXL [36], Flux [22], and pix2gestalt [34], which is the SOTA, from the five diverse image datasets. We put a red bounding box around a defective part for visualization purposes.

Using COCO-A [62] dataset, we show a side-by-side comparison in Fig. S1. The first row shows that pix2gestalt does not generate any part from the visible mask. The second and fifth rows show that pix2gestalt overestimates compared to our works. The third row shows that pix2gestalt fails to generate an occluded region, but ours can generate the missing pixel information. In the fourth row, the baseline ignores the scene context, which is a stretched arm, by putting a bent arm instead, while all of our methods successfully generate the stretched arm.

Similar issues from pix2gestalt are observed from BSDS-A [61] dataset, as shown in Fig. S2. The first, second, fourth, and fifth rows show the recurring overestimating issue while ours can generate similar to the ground truth. The third row shows that the missing pixel information still exists, while our work can predict the occluded regions.

In Fig. S3, we show examples from the KINS [37] dataset. From the third row, pix2gestalt covers most regions irrelevant to the visible mask. This dataset is not used in the original report in pix2gestalt, so the KINS dataset distribution might not be considered when constructing the training dataset, which shows the difficulties in designing customized datasets for robustness. On the other hand, our method is tuning-free and leverages the Internet-scaled pre-trained foundation models.

This issue remains for pix2gestalt when generating amodal masks in FishBowl [45] as shown in Fig. S4. The first and third rows still demonstrate overgrown issues from pix2gestalt generated amodal masks. The second and fifth rows still have missing pixel information, but our methods can predict the occluded regions. From the fourth row, when a visible mask is occluded heavily, the generated amodal mask from the baseline is a symmetrical shape. This dataset is not originally included in the report of pix2gestalt.

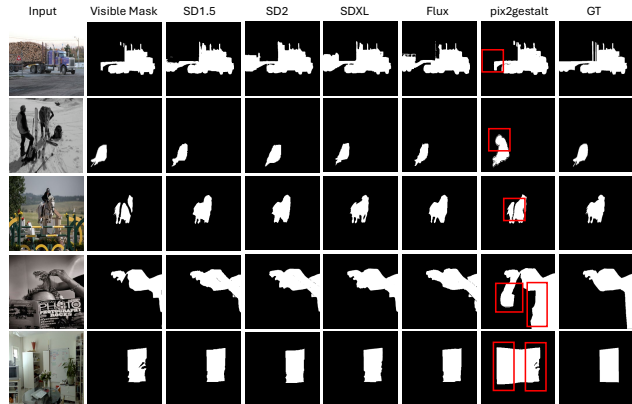


Figure S1. We show visual results of an amodal segmentation task based on COCO-A [62].

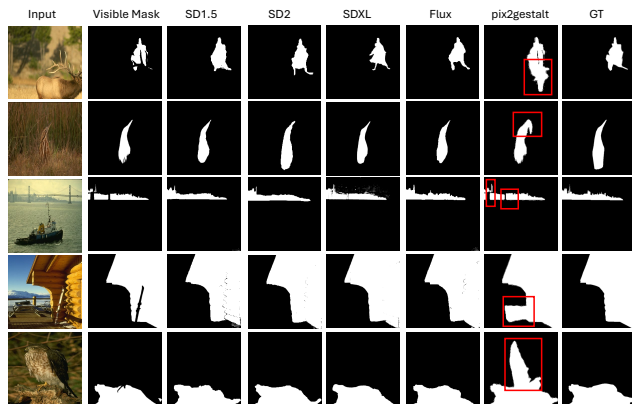


Figure S2. We show visual results of an amodal segmentation task based on BSDS-A [61].

SAILVOS [18] dataset reveals a new issue: hallucination. As we show in Fig. S5, all the rows show that pix2gestalt generates a random object that cannot be retrieved from the given scene. The fourth row shows the same category, which is a truck, but the details are not similar. While pix2gestalt constructs a customized dataset with 800k image pairs, it seems that pix2gestalt cannot cover all the occluded scenarios, while our tuning-free approach handles them well.

S2. Additional Ablation Study

Computation efficiency. We study the efficiency of our approach during the amodal mask generation compared to pix2gestalt. Tab. S1 reports the VRAM usage and infer-

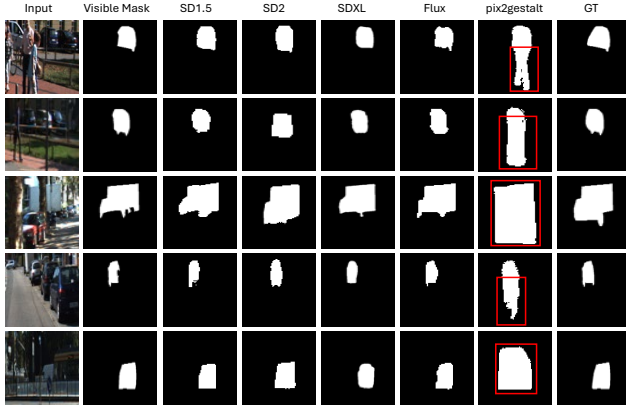


Figure S3. We show visual results of an amodal segmentation task based on KINS [37].

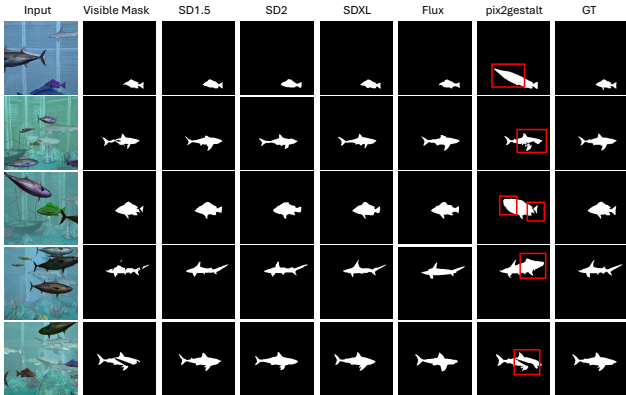


Figure S4. We show visual results of an amodal segmentation task based on FishBowl [45].

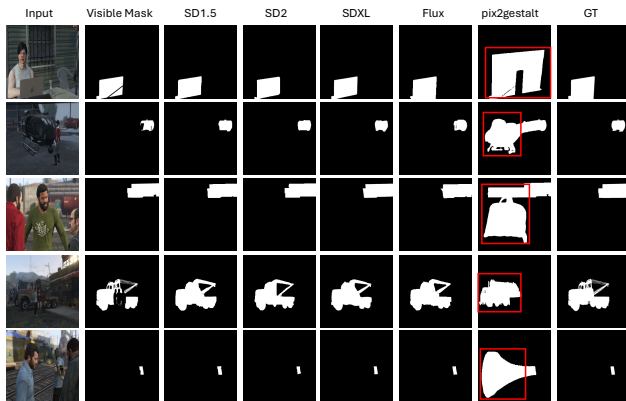


Figure S5. We show visual results of an amodal segmentation task based on SAILVOS [18].

ence time. The smallest model SD2 is $4.1\times$ more efficient in memory, and the inference (0.3 seconds) is $19\times$ faster compared to pix2gestalt [34]. Additionally, our best model (SDXL) is also more efficient than pix2gestalt.

	SD1.5 [40]	SDXL [36]	SD2 [43]	Flux [22]	pix2gestalt [34]
VRAM (GB) ↓	3.9	10.6	3.7	21.5	15.3
Inference (s) ↓	0.3	1.2	0.3	0.5	5.7

Table S1. We show peak GPU VRAM usage and inference time.

We first investigate further mIoU between the inpainting areas, M , and the ground truth amodal masks to validate our method by re-purposing the inpainting models to complete the missing pixel information. In Tab. S2, we show mIoU values from each dataset in different occlusion ranges. The mIoU difference between our best values and the mask coverage from each occlusion rate of all the datasets is 21.2%. Therefore, our proposed method generates a more accurate amodal mask than naively using the making area which takes unions of contours of visible masks as we explained.

To show that our proposed inpainting area method is effective, we create two additional mask baselines: 1) a naive bounding box style mask around the visible mask and 2) a depth-map-based mask using a deep learning-based monocular depth estimation [52], and those masks are presented as R , D , respectively. R is constructed with the smallest bounding box containing the visible mask of a target object to be inpainted. To generate D , we only include objects that are neighbors within 10 pixel-wise L2 distances from the target object. Then, we filter out any objects farther than the target object using the estimated depth map. Intuitively, we construct D that are close enough and objects that are in front of the target object, which causes an occlusion, in a certain range, r .

Using COCO-A [62], our proposed mask, M method generates 3.8% more accurate amodal masks on average from each occlusion rate as we shown in Tab. S3. Based on this dataset, when the occlusion rates are less than 50% and 40%, SD1.5 [40] with mask R and 40%, 30%, 20%, 10%, and 5% occlusion rates show that SDXL with mask D is the second-most accurate amodal mask. These trends continue with BSDS-A [61]. Our proposed mask, M , generates 1.6% better quality of amodal mask instead of using two masks R , D as shown in Tab. S4. Among using the two masks with different foundation models, Flux with mask D generates the second most accurate amodal mask when the objects are occluded less than 50% and 40%, and SDXL [36] with R works the second best when the occlusion rates are 30%, 20%, 10% and 5% or less. From Tab. S5 using KINS [37], we observed an interesting result that using a depth-aware mask, D , generates 5.0% more accurate amodal mask when the occlusion rates are 50%, 40%, 30%, and 20% or less compared to the method with mask M . When the objects are occluded 10%, 5% or less, mask M generates 6.1% more accurate amodal masks. In contrast to KINS [37], Tab. S6 shows mask M on FishBowl [45] predicts 2.3% more accurate amodal mask on average of six different occlusion rate ranges. The mask M performs bet-

Dataset	$\leq 50\%$	$\leq 40\%$	$\leq 30\%$	$\leq 20\%$	$\leq 10\%$	$\leq 5\%$
COCO-A [62]	66.5	67.7	68.8	69.6	71.4	71.6
BSDS-A [61]	75.2	75.1	75.0	74.4	73.5	73.7
KINS [37]	66.7	68.9	71.4	74.2	77.8	80.1
FishBowl [45]	59.4	59.7	60.0	60.1	60.4	60.7
SAILVOS [18]	30.0	30.2	30.4	30.8	31.0	30.9

Table S2. We evaluate mIoU($\%$) \uparrow with our inpainting area, M , and ground truth amodal segmentation masks from five different datasets among various occlusion rates from 50% to 5%.

DiffMod Mask	$\leq 50\%$	$\leq 40\%$	$\leq 30\%$	$\leq 20\%$	$\leq 10\%$	$\leq 5\%$
Ours M	82.7	85.4	88.0	90.6	93.6	95.0
SD1.5 R	77.7	80.0	82.1	84.1	86.9	88.2
SD1.5 D	75.6	78.1	80.4	82.7	85.8	87.3
SD2 R	75.4	77.7	79.8	81.8	84.5	85.6
SD2 D	75.8	78.2	80.4	82.7	85.6	86.9
SDXL R	76.7	79.5	82.0	84.6	87.7	88.9
SDXL D	77.0	80.0	82.5	85.1	88.6	90.6
Flux R	75.0	77.4	79.5	81.4	83.8	84.8
Flux D	76.8	79.3	81.5	83.7	86.4	87.5

Table S3. We evaluate our approach using COCO-A [62] with the other two masks approaches, (R , D), using mIoU($\%$) \uparrow .

DiffMod Mask	$\leq 50\%$	$\leq 40\%$	$\leq 30\%$	$\leq 20\%$	$\leq 10\%$	$\leq 5\%$
Ours M	78.3	80.5	82.8	85.8	88.9	90.7
SD1.5 R	74.8	77.8	80.4	83.1	86.0	87.6
SD1.5 D	74.7	77.6	80.3	83.2	86.2	87.9
SD2 R	75.6	78.4	80.8	83.2	85.6	87.2
SD2 D	75.0	77.5	79.9	82.4	84.6	86.2
SDXL R	75.0	78.4	81.3	84.5	87.7	89.1
SDXL D	74.7	77.4	79.9	82.6	85.7	87.4
Flux R	74.6	77.5	79.9	82.3	84.6	86.0
Flux D	76.2	78.8	81.0	83.2	85.6	86.3

Table S4. We evaluate our approach using BSDS-A [61] with the other two masks approaches, (R , D), using mIoU($\%$) \uparrow .

ter when the objects are occluded 40%, 30%, 20%, 10%, and 5% or less. Only SDXL [36] with mask D performs 0.2% better when the occlusion rate is 50% or less compared to the mask M . Tab. S7 shows that mask M generates 4.9% better quality of accurate amodal mask on all occlusion rate ranges compared to the masks R , D with other four foundation models including SD1.5 [40], SD2 [43], SDXL [36] and Flux [22].

S3. Implementation Details

Our implementation is based on Diffusers library version 0.31.0.dev0 from <https://github.com/huggingface/diffusers> and Flux inpainting from <https://github.com/Gothos/diffusers/>

DiffMod Mask	$\leq 50\%$	$\leq 40\%$	$\leq 30\%$	$\leq 20\%$	$\leq 10\%$	$\leq 5\%$
Ours M	64.8	66.2	68.2	70.6	74.1	77.3
SD1.5 R	60.7	61.8	63.2	64.9	67.5	70.7
SD1.5 D	63.5	64.8	66.5	68.6	71.7	74.8
SD2 R	61.7	62.7	63.9	65.4	67.6	70.7
SD2 D	63.4	64.4	65.8	67.5	69.9	72.9
SDXL R	46.8	48.4	50.9	54.1	60.2	69.1
SDXL D	60.4	62.1	66.6	70.8	67.3	70.5
Flux R	67.5	71.7	60.2	70.8	69.8	73.9
Flux D	70.7	74.8	69.1	75.1	72.3	77.0

Table S5. We evaluate our approach using KINS [37] with the other two masks approaches, (R , D), using mIoU($\%$) \uparrow .

DiffMod Mask	$\leq 50\%$	$\leq 40\%$	$\leq 30\%$	$\leq 20\%$	$\leq 10\%$	$\leq 5\%$
Ours M	80.4	82.8	85.3	88.0	90.7	91.9
SD1.5 R	60.9	63.0	65.0	67.3	70.4	74.3
SD1.5 D	79.7	81.1	82.9	84.4	85.9	86.3
SD2 R	72.5	74.6	76.6	78.6	80.4	81.1
SD2 D	74.1	76.3	78.6	81.1	83.4	84.7
SDXL R	76.9	79.2	81.6	83.8	85.8	86.7
SDXL D	80.6	82.1	84.0	85.3	86.8	86.8
Flux R	77.6	78.9	80.3	81.3	82.0	81.9
Flux D	64.1	65.4	67.3	69.5	72.7	75.6

Table S6. We evaluate our approach using FishBowl [9] with the other two masks approaches, (R , D), using mIoU($\%$) \uparrow .

DiffMod Mask	$\leq 50\%$	$\leq 40\%$	$\leq 30\%$	$\leq 20\%$	$\leq 10\%$	$\leq 5\%$
Ours M	80.0	82.3	84.1	85.8	87.4	88.8
SD1.5 R	67.5	69.4	70.8	72.2	74.0	76.1
SD1.5 D	65.6	67.4	68.8	70.5	72.3	74.6
SD2 R	68.2	69.8	71.2	72.7	75.5	77.3
SD2 D	69.7	71.4	72.8	74.5	77.1	78.8
SDXL R	57.4	59.0	60.6	62.5	65.6	67.6
SDXL D	63.5	65.1	66.6	68.2	70.7	72.3
Flux R	66.7	68.6	70.1	71.7	73.4	75.8
Flux D	76.1	77.8	79.2	80.5	81.9	83.6

Table S7. We evaluate our approach using SAILVOS [18] with the other two masks approaches, (R , D), using mIoU($\%$) \uparrow .

`tree/flux-inpaint` using Pytorch 2.4.1+cu124 and diffusion inpainting models from Hugging Face. The URL for SD15, SDXL, SD2 and Flux are

- <https://huggingface.co/benjamin-paine/stable-diffusion-v1-5-inpainting>,
- <https://huggingface.co/diffusers/stable-diffusion-xl-1.0-inpainting-0.1>,
- <https://huggingface.co/stabilityai/stable-diffusion-2-inpainting>
- <https://huggingface.co/black-forest-labs/FLUX.1-schnell>

To utilize Hugging face diffusion-based inpainting models,

we use `AutoPipelineForInpainting` module from the `Diffusers` library. Especially, we set `num_inference_steps` as 20, which is not a high value, since our goal is not generating photo-realistic quality images. All foundation models can fit into 24GB VRAM GPU, but we are unable to load Flux [22], so we apply 8-bit quantization using `optimum-quanto` from <https://github.com/huggingface/optimum-quanto>. We will release our implementation upon acceptance of this work.